applied sciences

MDPI

Article

Data-Driven Deformation Reliability of Retaining Structures in Deep Excavations Considering Measurement Error

Li Xu [1], Yang Xu [1], Cao Wang [1,2,3,*] and Kairui Feng [4]

1 College of Civil Engineering, Fuzhou University, Fuzhou 35018, Fujian, China; fzucivilxuli@fzu.edu.cn (L.X.); xu.ian.y@hotmail.com (Y.X.)
2 School of Civil Engineering, The University of Sydney, Sydney, NSW 2006, Australia
3 Department of Civil Engineering, Monash University, Clayton, VIC 3800, Australia
4 Department of Civil and Environmental Engineering, Princeton University, Princeton, NJ 08540, USA; kairuif@princeton.edu
* Correspondence: cao.wang@monash.edu

Received: 1 November 2019; Accepted: 10 December 2019; Published: 12 December 2019

Abstract: The deflections of retaining structures during deep excavation should be controlled below a predefined threshold in an attempt to mitigate the deformation-posed damage to the surrounding buildings and infrastructure facilities. In this paper, a new approach is presented to conducting deformation reliability assessments of retaining structures. The method is based on an extension of the classical first-passage reliability problem and is applied on the spatial scale of the retaining structures. With the proposed method, the in situ monitoring data and the associated measurement error can be easily incorporated, which accordingly improves the assessment accuracy. Moreover, the proposed method has a closed-form solution, which is beneficial for the computation efficiency and its practical application. The method was applied to assess the retaining structure reliability in a foundation excavation of a subway station in Fuzhou, China. The accuracy of the analytical results was verified through a comparison with those of Monte Carlo simulation. It was shown that the proposed method can represent well, the deformation-based safety level of retaining structures.

Keywords: deep excavation; deformation reliability; retaining structures; monitored data; measurement error; safety assessment

1. Introduction

The past decades have witnessed rapid growth in the number and scale of deep foundation pit projects in subway constructions around the world. Once a foundation pit accident (e.g., collapse of retaining structures) occurs, the consequence is often catastrophic, with ripple effects to the safety of adjacent buildings and underground pipelines [1–4]. In order to prevent such accidents, an important goal in the design and construction of foundation pits is to control the deformation of the soil and the retaining structures. Considering the uncertainties arising from the relevant parameters in the deformation process, the reliability approaches based on probability theory should be used to capture the randomness and variability of these parameters, yielding a probabilistic estimate of the safety level of the foundation excavations [5–9].

A significant number of studies are available in the literature regarding the deformation reliability assessment of retaining structures in foundation excavations. For example, Luo et al. [10] investigated the influence of statistical parameter uncertainty on the probability of serviceability failure in braced excavations based on the Bootstrap method. Wang et al. [11] conducted the probabilistic evaluation of serviceability failure in a braced excavation using the moment methods and the finite element

platform Plaxis^{TM}, and discussed the effect of spatial variability of soil parameters on the probability of serviceability failure. Goh and Kulhawy [12] calculated the reliability index of braced retaining walls by approximating the nonlinear limit state surface through a neural network model. Khosrojerdi et al. [13] evaluated the lateral deformation of geosynthetic reinforced soil walls and abutments based on some selected methods. Sayed et al. [14] studied the reliability of reinforced retaining walls based on finite element modeling. The response surface approach was utilized to represent the performance function, coupling the first order reliability method to compute the reliability index. Many of the existing studies have performed reliability assessments of retaining structures in foundation pits based on finite element software, where the computational cost could be dramatically high. Another approach is to establish a relationship between the retaining structure deformation and some key factors such as the wall deformation mode, wall stiffness, soil properties, adjacent building characteristics, and others [15–18]. However, these relationships are often empirically formulated and contain many unknown parameters to calibrate, which would become difficult in the presence of limited data and significant uncertainties. Alternatively, the direct use of in situ observed data could improve the accuracy and efficiency of structural reliability assessment [19–25]. For instance, Zhang et al. [22] investigated the impact of deep excavation on the adjacent metro shield tunnels using health monitoring data on the deformation. Qi and Zhou [24] developed a procedure for the Bayesian back-analysis of retaining wall reliability, making use of the deflection data monitored at multiple locations. However, the incorporation of measurement error (ME) associated with data collection [26,27] in the deformation reliability assessment of retaining structures has been limited discussed in previous studies. In fact, uncertain errors involved in the measurement of observations could deteriorate the quality of the data, and hence, the estimates of structural reliability [28–30].

This paper presents a method for deformation reliability analysis of retaining structures based on in situ monitoring data. The failure of a retaining structure is defined as a displacement at any depth exceeding the predefined threshold, which could differ from the engineering practice focusing on the deformations at the monitored depths only. By noting that the deformation distribution along the vertical direction of a retaining structure is a one-dimensional problem, this paper extends the classical first-passage reliability approach [31–33] from the temporal scale to the spatial scale. A closed-form solution is proposed for the deformation reliability assessment of retaining structures considering the potential failure risks at any depth. The impact of ME arising from data collection is explicitly incorporated in the proposed deformation reliability method. A case study is presented to demonstrate the applicability of the proposed method.

2. Deformation of Retaining Structures

The excavation of deep foundation pits in urban areas will inevitably result in the deformation of the soil and the retaining structures (e.g., retaining walls). Excessive deformation will trigger significant damage to adjacent buildings and infrastructure facilities. During the excavation process, the soil in the pit is removed and the earth pressure at the two sides of the retaining wall would be changed. The earth pressure on the outer side of the wall changes from static earth pressure to active earth pressure, and thus the difference in earth pressure between the inner and outer sides will lead to the horizontal deformation of the wall [34–36]. When the wall is supported at the top, as is often the case in engineering practice, the overall deformation of the wall along the vertical direction would behave in a "concave" way [37], as illustrated in Figure 1a (adopted from [38]).

A threshold for the lateral displacement is often used to determine the behaviour of the deformed retaining wall, which would be dependent on the excavation depth of the pit. When the deformation of the wall is monitored at some selected depths, the wall is deemed as *satisfactory* if all the monitored deformations do not exceed the predefined threshold, and vice versa. This method is relatively straightforward and reflects the current engineering practice for the performance evaluation of retaining structures in foundation pits, providing a simple yet useful tool for decision-makers. This approach only concerns the deformation at some certain depths (where monitored). In fact,

the failure of retaining walls (i.e., the displacement exceeds the threshold value) could occur at any depth. Illustratively, as shown in Figure 1b, even if all the displacements at the monitoring points are smaller than the limit, the actual displacement curve may still exceed the threshold, leading to the failure of retaining wall. Thus, a reliability assessment approach is essentially needed moving from "point control" to "surface control". Conceptually, increasing the number of monitoring points and inclinometers will increase the accuracy of the traditional point control-based method. While this idea could improve the monitoring practice in engineering, it is often difficult to implement due to the significant constraints of costs and monitoring equipment. This fact explains the motivation of the proposed "surface control" method.

In this paper, the deformation reliability of retaining structures are considered, which is defined as the probability that the maximum displacement of the retaining structure within the monitored area does not exceed the displacement limit. Suppose that there are n pieces of monitored deformation data at different depths $d_1, d_2, \ldots d_n$; namely, $y_1, y_2, \ldots y_n$ respectively. Let y_{lim} denote the predefined threshold for each y_i. The existing approach ("point control") simply concludes that the structural behavior is satisfactory if $y_{\text{lim}} \geq y_i$ for $\forall i = 1, 2, \ldots n$ and unsatisfactory otherwise. Clearly, the possible occurrence of *failure* (displacement exceeding limit) at locations rather than $\{d_1, d_2, \ldots d_n\}$ has been neglected. Also, the point control fails to take into account the ME associated with the monitored data. These disadvantages are addressed in this paper.

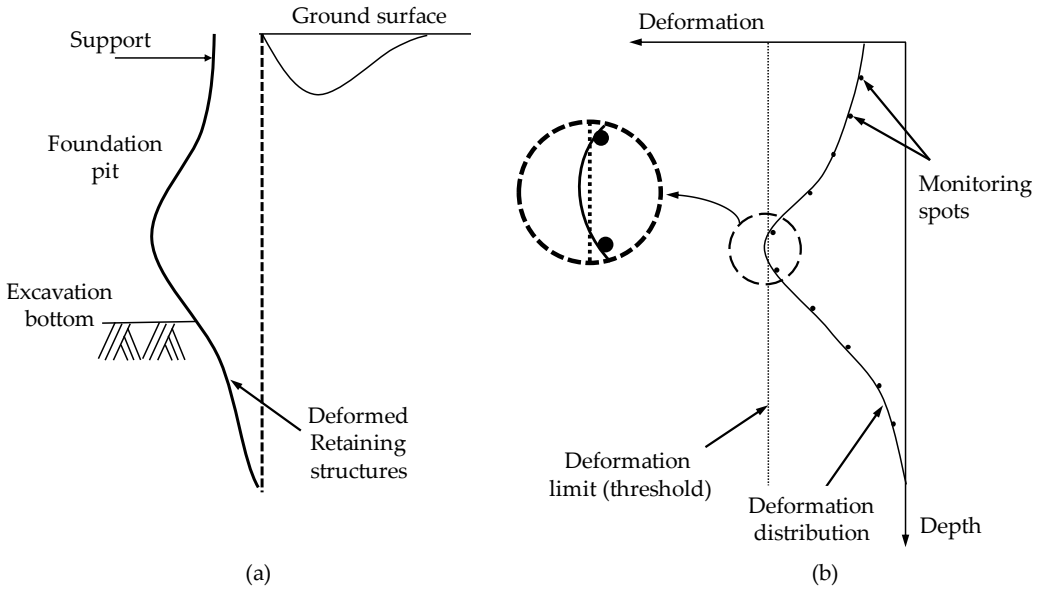

Figure 1. Illustration of deformed retaining structures in foundation pits. (**a**) Vertical deformation. (**b**) Failure occurring at unmonitored locations.

3. First-Passage Reliability Problem

3.1. Mathematical Basis

The classical first-passage reliability method was originally developed for time-dependent reliability analysis based on the stochastic process theory. The basic idea of the method is to assess the probability that the structural response does not exceed the safety limit for any time point within a reference period of $[0, T]$. Rice [39] proposed the first-passage calculation formula, which was used in structural dynamic reliability analysis. Siegert [40] developed an approach for the first-crossing probability based on the continuous Markov process. Helstrom and Isley [41] derived the analytical solution of the first-passage time using the Markov's envelope process. Coleman [42] proposed a Poisson approximation approach to calculate the crossing frequency. The Poisson approximation establishes the relationship between the crossing rate and the structural time-dependent reliability.

However, the computational accuracy depends on the assumption that the structural response exceeds the safety limit independently with a small probability. Cramér [43] showed that the solution to time-dependent reliability based on the Poisson process assumption is asymptotically accurate when the safety limit tends to infinity. Later on, the first-crossing reliability approach was extensively applied in the estimate of structural time-dependent safety level [31,32,44–46].

In this paper, the classical time-dependent reliability approach is extended, with some modifications, to estimate the deformation reliability of retaining structures, by noting that the spatial distribution of the deformation along the vertical direction is also a one-dimensional problem.

Mathematically, within a length of $[0, X]$ of interest, the limit state function $Z(x)$ takes the form of

$$Z(x) = R(x) - S(x), \tag{1}$$

where x denotes the location, $S(x)$ is the structural deformation at x, and $R(x)$ is the deformation limit at x. If $Z(x) \geq 0$ holds for all applicable $x \in [0, X]$, then the retaining structure is deemed as satisfactory. Typically, $R(x)$ can be treated as deterministic (or simply a constant in some occasions, e.g., y_{lim}, as discussed in Section 2). Taking into account the uncertainty associated with the process $S(x)$, the probability of $Z(x) \geq 0, \forall x \in [0, X]$ is the deformation reliability, denoted by

$$\mathbb{L}(X) = \mathbb{P}(Z(x) \geq 0, \forall x \in [0, X]), \tag{2}$$

where $\mathbb{P}(\,)$ is the probability of the event in the bracket. Recall that the traditional "point control" approach (c.f. Section 2) simply gives

$$\mathbb{L}_{\text{pc}}(X) = \mathbb{P}(Z(x) \geq 0, \forall x \in [0, X]) = \prod_{i=1}^{n} \mathbb{I}(y_i \geq y_{\text{lim}}), \tag{3}$$

where $\mathbb{I}(\,)$ is an indicative function, which returns 1 if the statement in the bracket is true and 0 otherwise.

Now we apply the first-passage reliability approach to estimate Equation (2). We assume that $S(x)$ is a weakly stationary Gaussian process. For the purpose of further derivation, we let

$$\Omega(x) = R(x) - \mathbb{E}(S(x)), \quad Y(x) = S(x) - \mathbb{E}(S(x)), \tag{4}$$

where $\mathbb{E}(\,)$ denotes the mean value of the variable in the bracket. With this, $Y(x)$ is a zero-mean stationary Gaussian process, as schematically shown in Figure 2. Thus, Equation (2) becomes

$$\mathbb{L}(X) = \mathbb{P}(\Omega(x) - Y(x) \geq 0, \forall x \in [0, X]). \tag{5}$$

The up-crossing rate of $Y(x)$ with respect to $\Omega(x)$ at location x, $\nu^+(x)$, is estimated according to

$$\begin{aligned} \lim_{\mathrm{d}x \to 0} \nu^+(x)\mathrm{d}x &= \Pr\left\{\Omega(x) > Y(x) \bigcap \Omega(x + \mathrm{d}x) < Y(x + \mathrm{d}x)\right\} \\ &= \Pr\left\{\Omega(x + \mathrm{d}x) - \dot{Y}(x)\mathrm{d}x < Y(x) < \Omega(x)\right\} \\ &= \int_{\dot{\Omega}(x)}^{\infty} \left[\dot{Y}(x) - \dot{\Omega}(x)\right] f_{Y\dot{Y}}\left[\Omega(x), \dot{Y}(x)\right] \mathrm{d}\dot{Y}(x)\mathrm{d}x \end{aligned}, \tag{6}$$

where $\dot{Y}(x)$ and $\dot{\Omega}(x)$ are the differentials of $Y(x)$ and $\Omega(x)$ respectively. Rearranging Equation (6) yields

$$\nu^+(x) = \int_{\dot{\Omega}(x)}^{\infty} \left(\dot{Y} - \dot{\Omega}\right) f_{Y\dot{Y}}\left(\Omega, \dot{Y}\right) \mathrm{d}\dot{Y}. \tag{7}$$

Since $Y(x)$ is a stationary Gaussian process, $Y(x)$ and $\dot{Y}(x)$ are mutually independent. Thus, it follows,

$$f_{Y\dot{Y}}(x,\dot{x}) = \frac{1}{2\pi\sigma_Y\sigma_{\dot{Y}}}\exp\left\{-\frac{1}{2}\left(\frac{x^2}{\sigma_Y^2}+\frac{\dot{x}^2}{\sigma_{\dot{Y}}^2}\right)\right\}, \tag{8}$$

where σ_Y and $\sigma_{\dot{Y}}$ are the standard deviations of $Y(x)$ and $\dot{Y}(x)$, respectively. Combining Equations (7) and (8) gives

$$\nu^+(x) = \frac{1}{2\pi\sigma_Y}\exp\left[-\frac{\Omega^2(x)}{2\sigma_Y^2}\right]\cdot\left\{\sigma_{\dot{Y}}\exp\left(-\frac{\dot{\Omega}^2(x)}{2\sigma_{\dot{Y}}^2}\right)-\sqrt{2\pi}\dot{\Omega}(x)\left[1-\Phi\left(\frac{\dot{\Omega}(x)}{\sigma_{\dot{Y}}}\right)\right]\right\}, \tag{9}$$

where $\Phi(\,)$ is the cumulative density function (CDF) of a standard normal distribution. Assume that the upcrossings of $Y(x)$ to $\Omega(x)$ are temporally independent and are rare, with which the Poisson process can be used to describe the occurrence of the upcrossings. Let N_X be the number of upcrossings within the length $[0, X]$, and it follows,

$$\Pr(N_X = i) = \frac{1}{i!}\left\{\int_0^X \nu^+(x)\mathrm{d}x\right\}^i \exp\left\{-\int_0^X \nu^+(x)\mathrm{d}x\right\}, \quad i = 0,1,2,\ldots. \tag{10}$$

By noting the fact that the structural deformation reliability within $[0, X]$ equals the probability of $N_X = 0$, one has

$$\mathbb{L}(X) = [1-\mathbb{P}(0)]\exp\left\{-\int_0^X \nu^+(x)\mathrm{d}x\right\}, \tag{11}$$

where $\mathbb{P}(0)$ is the failure probability (the probability of deformation exceeding the limit) at $x = 0$. Specifically, as $\mathbb{P}(0)$ is typically small enough, it follows that ([31–33])

$$\mathbb{L}(X) = \exp\left\{-\int_0^X \nu^+(x)\mathrm{d}x\right\}. \tag{12}$$

A similar form of Equation (12) (with the terms X and x denoting time) has been extensively used for the estimate of structural time-dependent reliability [31,32,44–46]. In this paper, Equation (12) is adopted with modifications to assess the deformation reliability of retaining structures.

Based on Equation (12), combining the concept of "point control", the deformation reliability, $\mathbb{L}_{\mathrm{nme}}(X)$, is formulated as follows,

$$\mathbb{L}_{\mathrm{nme}}(X) = \exp\left\{-\int_0^X \nu^+(x)\mathrm{d}x\right\}\cdot\prod_{i=1}^{n}\mathbb{I}(y_i \geq y_{\mathrm{lim}}). \tag{13}$$

By comparing Equations (3) and (13), it can be seen that the proposed method in Equation (13) has moved the deformation limit state from "point control" to "surface control". Note that the subscript "nme" in Equation (13) means that $\mathbb{L}_{\mathrm{nme}}(X)$ has not (n) considered the measurement (m) error (e). The impact of ME on the deformation reliability is addressed later, in Section 4.3.

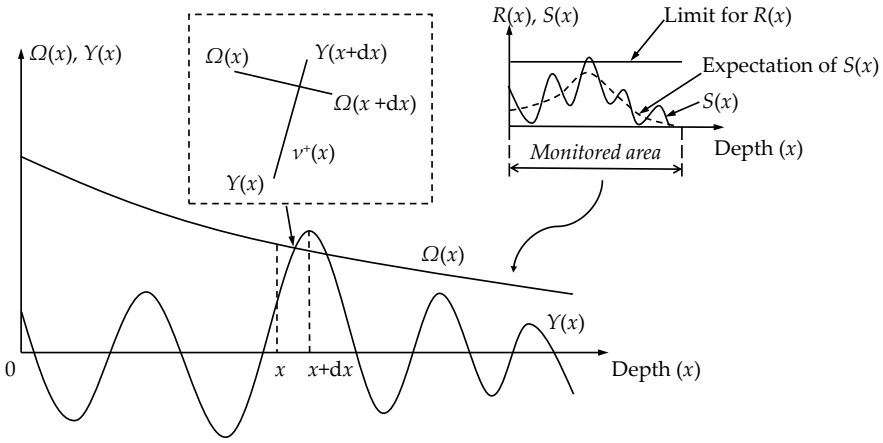

Figure 2. Location-dependent $\Omega(x)$ and $Y(x)$.

3.2. Parameter Calibration Using Observational Data

The deformation monitoring data is a set of discrete samples of a random sequence that varies with depth. Note that the relevant parameters (c.f. $\Omega(x)$ and $Y(x)$ in Equation (13)) involved in the first-passage reliability problem are continuous along the depth x. This section presents a method for calibrating these quantities by regression analysis of the samples.

3.2.1. Fitting $\Omega(x)$ and Subsequently Obtaining $\dot{\Omega}(x)$

The retaining wall deformation caused by foundation pit excavation varies with the construction stage. The damage to adjacent buildings due to pit excavation at the early stages has been rarely reported but occurs mainly at the latter stages [5,47]. Therefore, the emphasis could be put on the deformation reliability assessment of retaining structures at the later stages of foundation pit excavation. In the presence of a sequence of observed deformation data, taking the depth x as the argument, the (continuous) deformation with respect to x can be fitted with an m-degree polynomial as follows,

$$\mathbb{E}(S(x)) = \sum_{i=0}^{m} \gamma_i x^i, \tag{14}$$

where γ_i is the coefficient of the polynomial. In order to avoid Runge's phenomenon in the fitting [48] (the oscillation at the edge of the interval when using a high-order polynomial interpolation), the degree m should be carefully selected. Furthermore, one can obtain $\Omega(x)$ according to Equation (4), and further $\dot{\Omega}(x)$ by differentiating $\Omega(x)$.

3.2.2. Fitting the Variance of $Y(x)$

With Equation (4) and a similar form of Equation (14), one can fit $\mathbb{E}(Y(x))$ based on the discrete observed data $y_1, y_2, \ldots y_n$ at depths $d_1, d_2, \ldots d_n$. Furthermore, employing the concept of "average variance" [49], the variance of $Y(x)$ is computed as follows,

$$\mathbb{V}(Y(x)) = \mathbb{E}\{[Y - \mathbb{E}(Y)]^2\} = \frac{1}{n}\sum_{i=1}^{n}(y_i - \widetilde{Y}(d_i))^2, \tag{15}$$

where $\mathbb{V}(\,)$ represents the variance of the random variable in the bracket, and $\widetilde{Y}(d_i)$ is the deformation response evaluated at depth d_i with the fitted function $Y(x)$. The standard deviation of $Y(x)$, σ_Y, is then simply the square root of the variance.

3.2.3. Fitting the Variance of $\dot{Y}(x)$

Based on the monitored deformation data $y_1, y_2, \ldots y_n$ at depths $d_1, d_2, \ldots d_n$, the samples of $\dot{Y}$ are first approximated by $\left\{\frac{y_{i+1}-y_i}{d_{i+1}-d_i}\right\}$ for $i = 0, 1, 2, \ldots n-1$, where $y_0 = 2y_1 - y_2$ and $d_0 = 2d_1 - d_2$. With this, $\mathbb{E}(\dot{Y}(x))$ is fitted using a polynomial expression similar to Equation (14). Subsequently, by referring to Equation (15), the variance of $\dot{Y}(x)$ is determined by

$$\mathbb{V}(\dot{Y}) = \mathbb{E}\{[\dot{Y} - \mathbb{E}(\dot{Y})]^2\} = \frac{1}{n}\sum_{i=1}^{n}\left(\frac{y_i - y_{i-1}}{d_i - d_{i-1}} - \widetilde{\dot{Y}}(d_i)\right)^2, \tag{16}$$

where $\widetilde{\dot{Y}}(d_i)$ is the fitted function $\dot{Y}(x)$ evaluated at depth d_i.

3.2.4. Test of Fitting Accuracy

In order to evaluate the accuracy of the fitting-based prediction of the quantities, the coefficient of determination (R-square) is a frequently-used tool [50], which is computed as follows,

$$R^2 = 1 - \frac{\sum_{i=1}^{n}(y_i - \widetilde{y}_i)^2}{\sum_{i=1}^{n}(y_i - \bar{y})^2}, \tag{17}$$

where $\widetilde{y}_i$ is the fitted value, and $\bar{y} = \frac{1}{n}\sum_{i=1}^{n} y_i$. This coefficient varies within $[0, 1]$. A value of R^2 approaching 1 indicates a well-fitted prediction model.

4. Reliability Assessment Considering ME

4.1. Measurement of Retaining Structure Deformation

An inclinometer system is often used to measure the deformation of retaining walls in practical engineering, which typically comprises a sensor probe, a load-bearing cable with a scaler, and a reader, as illustrated in Figure 3a,b. The sensor probe is a key component for the lateral displacement measurement in the inclinometer. A high-precision acceleration digital sensor is installed inside the probe. The tilt of the casing in four different directions, namely, A_0, A_{180}, B_0 and B_{180} in Figure 3b, is measured by the probe. Two sets of guide wheels are located at the upper and lower parts of the probe respectively, with which the probe can slide up and down inside the inclinometer casing (c.f. Figure 3c).

The basic idea to measure the horizontal displacement with an inclinometer is to first determine the azimuth between the central axis of the inclinometer and the vertical line of the gravity pendulum in the probe, and then to use the geometric relationship (c.f. Figure 3d) to compute the accumulative displacement at different depths [51–53]. Let the inclination angle measured at a certain depth be α, and L the overstep (measurement interval), as shown in Figure 3d. With this, the horizontal displacement at this depth, δ, is computed by $\delta = L\sin\alpha$ according to the triangular relationship. Furthermore, calculating the horizontal offset from the bottom to the top, the lateral displacement at the jth measurement interval relative to the bottom, D_j, is determined by

$$D_j = \sum_{i=1}^{j}\delta_i = \sum_{i=1}^{j} L\sin\alpha_i \tag{18}$$

where α_i is the angle between the central axis of the inclinometer and the vertical line of the gravity pendulum at the ith measurement interval and δ_i is the horizontal offset at the ith interval.

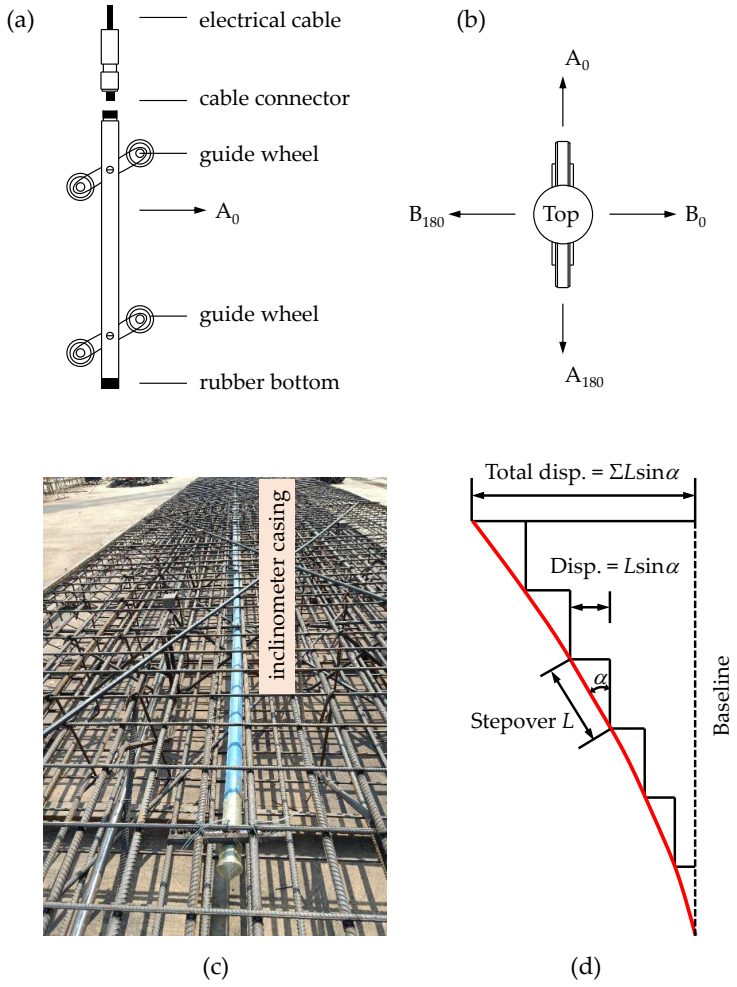

Figure 3. Inclinometers used to measure the lateral displacement of retaining walls. (**a**,**b**) Elevation and top view of a typical inclinometer probe [54]. (**c**) A tube (PVC plastic, ABS plastic or aluminium) is installed serving as the inclinometer casing for the purpose of ground measurement. (**d**) Measurement of lateral displacement [51].

4.2. Sources of ME

The ME inevitably arises from the observed data in practice. In terms of the lateral displacement data monitored by an inclinometer, the ME could be caused by inclinometer accuracy and human error. The former consists of bias-shift error, sensitivity drift, rotation error, depth positioning error and others [51,55,56]. For example, the bias-shift error (also known as zero-shift error) is due to the initial checksum at the probe (c.f. A_0 and A_{180} in Figure 3b) not being zero. Ideally, the sum of the readings of A_0 and A_{180} should be zero with identical numbers but opposite signs. However, there is often a slight bias at the initial readings due to the imperfection of the probe. Details for other types of ME can be found elsewhere [51,55]. It was argued in [51] that the systematic error due to inclinometer accuracy, which accumulates arithmetically with the number of measurement intervals, is more important and significant than the random error (human error). As such, in this paper, only the ME due to inclinometer accuracy is considered. Taking into account its randomness by nature, the ME is represented by a random variable. The impact of ME on the deformation reliability of retaining structures is formulated in the next Section.

4.3. Deformation Reliability Incorporating ME

Recall Equation (13), which gives the deformation reliability of retaining structures without considering the potential impact of ME. Taking into account the systematic error in the measurement of lateral displacement, which dominates in ME [51], we let Δ_i denote the error associated with the ith (from the bottom to the top) measurement interval, which is a random variable representing the uncertainty of the measurement. Since the monitored data at different depths are obtained with the same inclinometer, and the ME accumulates with the number of measurement intervals, it is reasonable to assume that each Δ_i is fully correlated and follows a normal distribution. With this, it follows that

$$\Delta_i = k_i \epsilon, \quad i = 1, 2, 3, \dots n, \tag{19}$$

where ϵ is a random variable that reflects the accuracy of the inclinometer, and k_i is a scaler ($i = 1, 2, \dots n$) that reflects the accumulation of the ME with the number of measurement intervals. With Equation (19),

$$\sigma_{\Delta_i} = k_i \sigma_\epsilon, \tag{20}$$

where $\sigma_\bullet$ denotes the standard deviation of $\bullet = \Delta_i$ and ϵ. Let A denote the accuracy of the inclinometer. With a confidence level of 95%, it follows that

$$2\sigma_{\Delta_i} = Ad_i \Rightarrow \sigma_{\Delta_i} = \frac{Ad_i}{2}. \tag{21}$$

Notice that the coefficient "2" in Equation (21) is explained by the 95% confidence level; that is, $\Phi(2) - \Phi(-2) \approx 95\%$. Similarly, if the confidence level is 99%, then the coefficient "2" should be replaced by $\Phi^{-1}(1 - 99\%) \approx 2.58$.

Combing Equations (20) and (21) gives

$$\frac{Ad_i}{2} = k_i \sigma_\epsilon \Rightarrow k_i = \frac{Ad_i}{2\sigma_\epsilon}. \tag{22}$$

Furthermore, in the presence of ME, the application of "point control" (c.f. Section 2 and Equation (3)) gives

$$\begin{aligned} \mathbb{L}_{\text{pc}}(X) &= \mathbb{P}\left(y_1 + \Delta_1 \le y_{\lim} \cap y_2 + \Delta_2 \le y_{\lim} \cap \dots y_n + \Delta_n \le y_{\lim}\right) \\ &= \mathbb{P}\left(y_1 + k_1\epsilon \le y_{\lim} \cap y_2 + k_2\epsilon \le y_{\lim} \cap \dots y_n + k_n\epsilon \le y_{\lim}\right) \\ &= \mathbb{P}\left(\epsilon \le \frac{y_{\lim} - y_1}{k_1} \cap \epsilon \le \frac{y_{\lim} - y_2}{k_2} \cap \dots \epsilon \le \frac{y_{\lim} - y_n}{k_n}\right) \\ &= \Phi\left(\frac{\min\limits_{i=1}^{n} \frac{y_{\lim} - y_i}{k_i}}{\sigma_\epsilon}\right) \overset{\text{Equation (22)}}{=\!=\!=} \Phi\left(2 \min_{i=1}^{n} \frac{y_{\lim} - y_i}{Ad_i}\right) \end{aligned}. \tag{23}$$

Clearly, if $y_{\lim} - y_i \ge 0$ for $\forall i = 1, 2, \dots n$ and $A \to 0$ (i.e., infinite accuracy) in Equation (23), then $\mathbb{L}_{\text{pc}}(X) \to 1$. On the other hand, if $\min(y_{\lim} - y_i) < 0$ and $A \to 0$, then $\mathbb{L}_{\text{pc}}(X) \to 0$. These facts imply that Equation (23) is a generalized case of Equation (3). Furthermore, similar to Equation (13), the deformation reliability in the presence of ME is formulated as follows,

$$\mathbb{L}_{\text{me}}(X) = \exp\left\{-\int_0^X \nu^+(x)\mathrm{d}x\right\} \cdot \Phi\left(2 \min_{i=1}^{n} \frac{y_{\lim} - y_i}{Ad_i}\right). \tag{24}$$

The comparison between Equations (13) and (24) shows that the measurement accuracy of the inclinometer (A) has been explicitly incorporated in the deformation reliability of retaining structures. The applicability and accuracy of Equation (24) is demonstrated in the following.

Notice that the proposed method (Equation (13) or (24)) only needs the computational costs of calculating a one-fold integral, which enables the deformation reliability assessment to be performed efficiently compared with the traditional finite element-based approaches. Thus, the proposed method is promising to be adopted for use in practical engineering.

5. Case Study

5.1. Background

The deep foundation pit project of a subway station considered in this Section is located in Changle District, Fuzhou, China. It is a two-story, double-column, and three-span station with a length of 293 m and a width of 21.7 m. The total construction area of the station is 17,861.2 m^2. The station was constructed with the cut-and-cover method. The retaining structure is a 800 mm-thick continuous wall. The layout of the monitoring points is shown in Figure 4a, where the black dots labeled with "QCX" are the monitored locations. Figure 4b presents a photo from the in-situ construction, where the reinforced concrete supports are used at the top of the excavation and steel supports are used elsewhere.

The CX-06B inclinometer was used in this project to measure the deformation of retaining walls. The CX-06B inclinometer is a geotechnical instrument equipped with a high-precision accelerometer. It has been widely used in the measurements of lateral displacements for building foundations, mines, foundation pit excavation, and underground structures. The major technical features of CX-06B are as summarized in Table 1.

Table 1. Features of the inclinometer used in the project.

Item	Description
Resolution	0.02 mm/500 mm
Measurement range	−50°∼+50°
Accuracy	±4 mm/15 m
Minimum stepover	500 mm
Surrounding temperature	−10 °C∼+50 °C

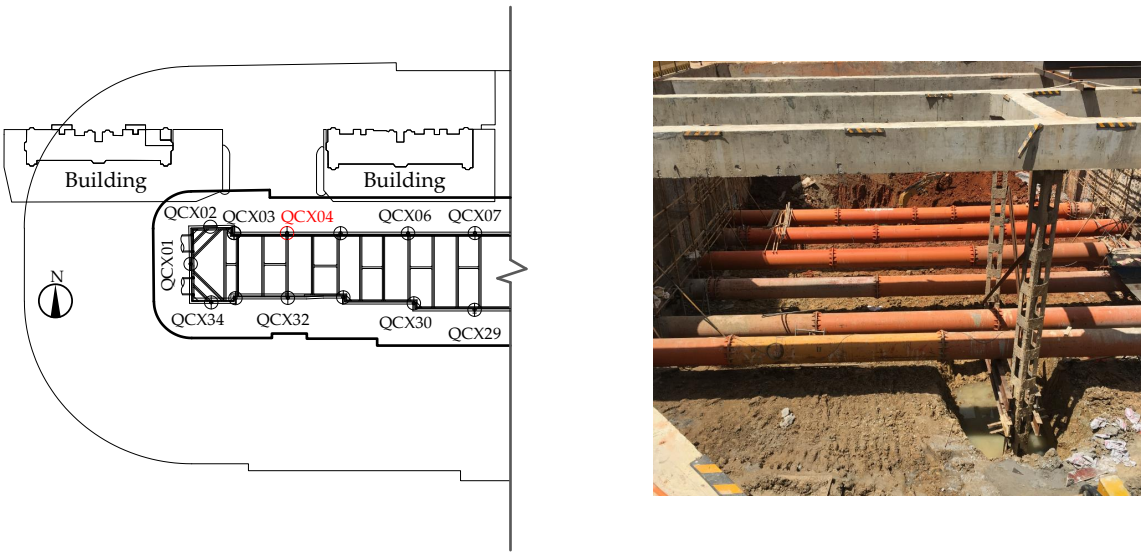

Figure 4. Foundation pit excavation of a subway station. (**a**) Layout. (**b**) *In-situ* photo.

5.2. Deformation Reliability Assessment

We illustratively chose the monitored data at location QCX04 (c.f. Figure 4a) to perform deformation reliability assessment. The horizontal displacements measured at different depths on each day are shown in Table 2. Note that the depths in Table 2 were calculated from the bottom, which would equal 43.5 m at the top (ground surface).

The fitting of $\mathbb{E}(S(x))$ is performed using a polynomial, with which $\Omega(x)$ and $Y(x)$ in Equations (13) and (24) can be subsequently determined. The fitting accuracy is evaluated by the determination coefficient R^2 in Equation (17). Using the monitoring data from the subset of 1/4–3/4 of the depth, the dependence of R^2 on the order of polynomial (c.f. the term m in Equation (14)) is shown in Figure 5. It can be seen that when $m \geq 2$, $R^2 > 0.9$, fairly close to 1. While a greater value of m will lead to a greater value of R^2, the Runge's phenomenon could occur as m is sufficiently large. Thus, m was chosen as 4 for the following analyses. Furthermore, assuming that the displacement limit $R(x)$ is 73.5 mm, $\Omega(x)$ can be determined according to Equation (4). The derivative of $\Omega(x)$ gives $\dot{\Omega}(x)$. The variances of both $Y(x)$ and $\dot{Y}(x)$ were computed with Equations (15) and (16). With this, the deformation reliability was found to be $\mathbb{L}_{\text{nme}}(43.5) = 0.956$ according to Equation (13). That is, the probability that the maximum lateral displacement of the retaining wall at location QCX04 does not exceed the predefined limit is 95.6%.

Next, the impact of ME on the deformation reliability is discussed. As introduced in Table 1, the inclinometer CX-06B used in this project has a measurement accuracy of $A = 4$ mm/15 m $= 2.667 \times 10^{-4}$. With this, applying Equation (23) yields $\mathbb{L}_{\text{pc}}(43.5) = 0.518$. Furthermore, with Equation (24), the deformation reliability taking into account the impact of ME is estimated as $\mathbb{L}_{\text{me}}(43.5) = 0.956 \times 0.518 = 0.495$. That is, in the presence of ME, the probability that the maximum lateral displacement of the retaining wall at location QCX04 does not exceed the predefined limit decreases to 49.5%. This implies that ignoring the impact of ME could significantly overestimate the deformation reliability of retaining structures.

Table 2. Cumulative deformations (CDs) at different depths for location QCX04.

Depth (m)	CD (mm)	Depth (m)	CD (mm)	Depth (m)	CD (mm)	Depth (m)	CD (mm)
1.0	−4.62	12.0	37.48	23.0	58.03	34.0	4.97
1.5	−3.63	12.5	41.22	23.5	54.29	34.5	4.46
2.0	−2.43	13.0	44.99	24.0	50.86	35.0	4.19
2.5	−1.69	13.5	49.04	24.5	47.90	35.5	3.76
3.0	−0.07	14.0	52.64	25.0	44.40	36.0	3.03
3.5	1.62	14.5	56.20	25.5	40.07	36.5	2.64
4.0	2.98	15.0	59.43	26.0	36.37	37.0	2.30
4.5	4.10	15.5	62.56	26.5	32.87	37.5	1.90
5.0	5.73	16.0	65.44	27.0	28.97	38.0	1.80
5.5	1.08	16.5	68.09	27.5	25.56	38.5	1.76
6.0	3.44	17.0	70.11	28.0	22.40	39.0	1.56
6.5	4.41	17.5	71.69	28.5	19.40	39.5	1.31
7.0	5.94	18.0	72.81	29.0	16.54	40.0	1.27
7.5	8.05	18.5	73.35	29.5	14.28	40.5	0.94
8.0	10.87	19.0	72.80	30.0	12.58	41.0	0.65
8.5	13.73	19.5	72.45	30.5	10.76	41.5	0.33
9.0	16.62	20.0	71.27	31.0	9.23	42.0	0.30
9.5	19.67	20.5	69.77	31.5	8.05	42.5	0.25
10.0	22.94	21.0	68.01	32.0	7.32	43.0	0.34
10.5	26.36	21.5	66.21	32.5	6.62	43.5	0.17
11.0	30.13	22.0	64.05	33.0	6.11		
11.5	33.71	22.5	61.22	33.5	5.61		

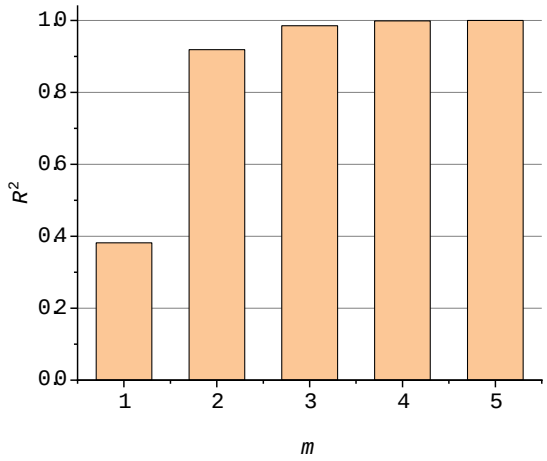

Figure 5. Dependence of the *R*-squared on the fitting order (c.f. m in Equation (14)).

5.3. Verification of the Proposed Method

In order to verify the accuracy of the proposed method in Equation (24), the Monte Carlo simulation method is used. The analytical and simulated reliabilities are expected to agree well with each other to demonstrate the applicability of Equation (24). The basic idea of the simulation-based approach is to generate a set of random lateral displacements distributed along the vertical direction of the retaining wall, and compare each of them with the predefined threshold to determine the structural state (failure or survival). For the jth simulation run ($j = 1, 2, \ldots q$, where q is sufficiently large), the procedure is summarized as follows.

1. Let $r_j = 1$, which becomes 0 if the jth sampled scenario of lateral deformation leads to structural failure (i.e., maximum lateral displacement exceeds the threshold).
2. Calculate the displacement distribution along the vertical direction of the retaining wall at an interval of 5 mm (excluding the monitoring points) using Equation (14).
3. Generate a set of correlated zero-mean normal random variables with a standard deviation of σ_Y using the Nataf transformation method [32], and add them to the sample values from Step 2 respectively. This is to obtain a set of displacement values that are approximately continuous along the depth and have the same statistical characteristics as those used in the analytical approach.
4. Sample a realization of normally distributed ϵ with a mean value of 0 and a standard deviation of σ_ϵ. Use Equation (22) to compute k_i and subsequently utilize Equation (21) to calculate each Δ_i, where $i = 1, 2, \ldots n$.
5. The sampled data at depth d_i is calculated as $y_i + \Delta_i$ for $i = 1, 2, \ldots n$.
6. Combining those sampled data in Steps 3 and 5, for each of them, if the displacement exceeds the predefined limit, then set $r_j = 0$.
7. Record r_j.

With q simulation runs, the simulated deformation reliability is approximated by $\frac{1}{q}\sum_{j=1}^{q} r_j$.

The analytical and simulation-based reliabilities with different displacement thresholds are presented in Figure 6 for the purposes of comparison. The number of simulation runs is $q = 10^6$ for each case. It can be seen that at the upper tail (e.g., ≥ 73 mm), the results from both approaches agree well with each other, which indicates the accuracy of the proposed method in Equation (24). At the lower tail, the reliability associated with the analytical approach is slightly greater than that of the simulation-based approach due to the impact of Poisson assumption in the analytical formulation (c.f. Section 3.1). Nonetheless, as the emphasis is on the behavior at the upper tail for most engineering cases, the proposed reliability assessment method in Equation (24) can be used to reasonably estimate the deformation safety level of retaining structures.

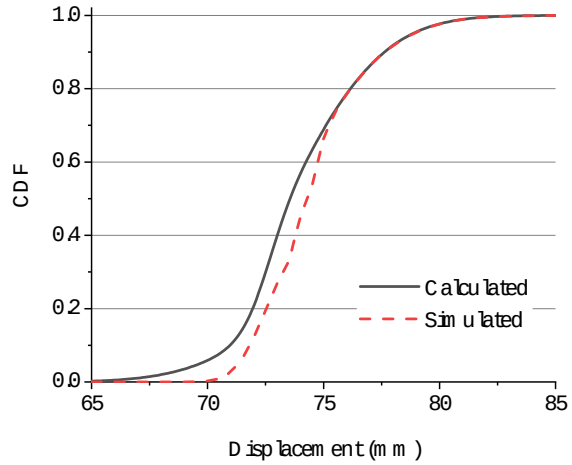

Figure 6. Verification of the method in Equation (24).

5.4. Discussions

The deformation reliability approach in Equation (13) based on the crossing rate model takes into account the potential failures at the depths rather than the monitored ones, and thus yields a reliability method that moves from "point control" to "surface control". Using the monitored data for location QCX04 in Table 2, the dependence of deformation reliability on the displacement limit is presented in Figure 7. The maximum monitored displacement is 73.35 mm according to Table 2. Correspondingly, in Figure 7, the deformation reliability equals 0 if the displacement limit is smaller than 73.35 mm. On the other hand, when $R(x) \geq 73.35$ mm, the deformation reliability increases from 95.6% to 1. This means that the conventional "point control" may overestimate the deformation reliability by simply focusing on the deformations at limited points.

Furthermore, taking into account the impact of ME, the deformation reliability is also shown in Figure 7 for the purpose of comparison. Clearly, the dependence of $\mathbb{L}_{\text{me}}$ in Equation (24) on the displacement threshold is smoother compared with $\mathbb{L}_{\text{nme}}$. For cases where $\mathbb{L}_{\text{nme}} > 0$ (that is, $\min(y_{\text{lim}} - y_i) \geq 0$), it can be seen that $\mathbb{L}_{\text{me}} < \mathbb{L}_{\text{nme}}$. This can be explained by noting that in Equations (13) and (24), $\left(2\min_{i=1}^{n} \frac{y_{\text{lim}} - y_i}{Ad_i}\right) < \prod_{i=1}^{n} \mathbb{I}(y_i \geq y_{\text{lim}}) = 1$, which gives $\mathbb{L}_{\text{me}} < \mathbb{L}_{\text{nme}}$. This comparison again suggests the important role of ME in the deformation reliability of retaining walls.

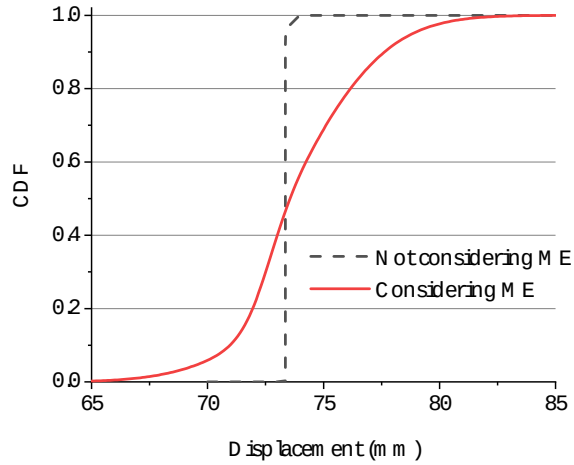

Figure 7. Cumulative density functions (CDFs) of the maximum displacement computed with Equations (13) and (24).

6. Conclusions

In this study, a new approach was developed for the deformation reliability analysis of retaining structures in deep excavations, making use of the in situ monitored data. The method expands the classical first-passage based time-dependent reliability problem into the spatial scale, and explicitly incorporates the potential impact of measurement error. The new method considers the deformation scenario of the whole structure rather than limited points, and thus moves from the conventional "point control" method to "surface control". The proposed method only involves the calculation of a one-fold integral, with which the deformation reliability assessment can be conducted efficiently compared with the traditional finite element-based approaches. An illustrative example is presented in this paper to demonstrate the applicability of the proposed method. The following conclusions can be drawn from this paper.

1. The accuracy and applicability of the proposed deformation reliability method were verified by comparing the results with those obtained from a Monte Carlo simulation.
2. If only taking into account the deformations at the depths monitored, the deformation reliability of retaining structures could be overestimated, due to the potential failures at the non-monitored points.
3. If ignoring the impact of ME, the deformation reliability could be overestimated significantly if the deformation scenario passes the "point control" examination. This suggests the importance of carefully identifying the measurement error of the equipment (inclinometer) in an attempt to achieve a reliable estimate of the safety level of retaining structures.

The proposed method can be further extended for the deformation reliability assessment of excavation surfaces containing multiple retaining structures. Further work is underway regarding the deformation reliability assessment of deep excavations on both the spatial and the temporal scales.

Author Contributions: Conceptualization, L.X. and C.W.; methodology, Y.X. and C.W.; analysis, Y.X.; drafting and editing, L.X., Y.X., C.W., and K.F.; supervision, L.X. and C.W.; funding acquisition, L.X.

Funding: This research was funded by the Science and Technology Bureau of Fuzhou, China (grant number 2018-G-88) and the Provincial Department of Science and Technology of Fujian, China (grant number 2017J01698).

Conflicts of Interest: The authors declare no conflict of interest.

References

1. Zhou, H.; Zhang, H. Risk assessment methodology for a deep foundation pit construction project in Shanghai, China. *J. Constr. Eng. Manag.* **2011**, *137*, 1185–1194. [CrossRef]
2. Chai, J.; Shen, S.; Ding, W.; Zhu, H.; Carter, J. Numerical investigation of the failure of a building in Shanghai, China. *Comput. Geotech.* **2014**, *55*, 482–493. [CrossRef]
3. Ahmed, S.M.; Fayed, A.L. Mitigation of Risks Associated with Deep Excavations: State of the Art Review. In Proceedings of the Industry Academia Collaboration (IAC 2015), Cairo, Egypt, 6–8 April 2015.
4. Zhou, Y.; Su, W.; Ding, L.; Luo, H.; Love, P.E. Predicting safety risks in deep foundation pits in subway infrastructure projects: Support vector machine approach. *J. Comput. Civ. Eng.* **2017**, *31*, 04017052. [CrossRef]
5. Tang, Y. Probability-based method using RFEM for predicting wall deflection caused by excavation. *J. Zhejiang Univ. Sci. A* **2011**, *12*, 737–746. [CrossRef]
6. Papaioannou, I.; Straub, D. Reliability updating in geotechnical engineering including spatial variability of soil. *Comput. Geotech.* **2012**, *42*, 44–51. [CrossRef]
7. Goh, A.T.; Xuan, F.; Zhang, W. Reliability assessment of diaphragm wall deflections in soft clays. In *Foundation Engineering in the Face of Uncertainty: Honoring Fred H. Kulhawy*; American Society of Civil Engineers: Reston, VA, USA, 2013; pp. 487–496.
8. Tang, X.S.; Li, D.Q.; Zhou, C.B.; Phoon, K.K. Copula-based approaches for evaluating slope reliability under incomplete probability information. *Struct. Saf.* **2015**, *52*, 90–99. [CrossRef]
9. Luo, Z.; Li, Y.; Zhou, S.; Di, H. Effects of vertical spatial variability on supported excavations in sands considering multiple geotechnical and structural failure modes. *Comput. Geotech.* **2018**, *95*, 16–29. [CrossRef]

10. Luo, Z.; Atamturktur, S.; Juang, C.H. Bootstrapping for characterizing the effect of uncertainty in sample statistics for braced excavations. *J. Geotech. Geoenviron. Eng.* **2012**, *139*, 13–23. [CrossRef]
11. Wang, L.; Luo, Z.; Gong, W.; Khoshnevisan, S.; Juang, C.H. Moment methods for assessing the probability of serviceability failure in braced excavations. In Proceedings of the Geo-Congress 2014: Geo-Characterization and Modeling for Sustainability, Atlanta, GA, USA, 23–26 February 2014; pp. 3293–3302.
12. Goh, A.; Kulhawy, F. Reliability assessment of serviceability performance of braced retaining walls using a neural network approach. *Int. J. Numer. Anal. Methods Geomech.* **2005**, *29*, 627–642. [CrossRef]
13. Khosrojerdi, M.; Xiao, M.; Qiu, T.; Nicks, J. Evaluation of prediction methods for lateral deformation of GRS walls and abutments. *J. Geotech. Geoenviron. Eng.* **2016**, *143*, 06016022. [CrossRef]
14. Sayed, S.; Dodagoudar, G.; Rajagopal, K. Finite element reliability analysis of reinforced retaining walls. *Geomech. Geoengin. Int. J.* **2010**, *5*, 187–197. [CrossRef]
15. Goldberg, D.; Jaworski, W.; Gordon, M. *Lateral Support Systems and Underpinning*; Technical report, DC Report FHWA-RD-75-128; Federal Highway Administration: Washington, DC, USA, 1976.
16. Ou, C.Y.; Hsieh, P.G.; Chiou, D.C. Characteristics of ground surface settlement during excavation. *Can. Geotech. J.* **1993**, *30*, 758–767. [CrossRef]
17. Finno, R.J.; Voss, F.T., Jr.; Rossow, E.; Blackburn, J.T. Evaluating damage potential in buildings affected by excavations. *J. Geotech. Geoenviron. Eng.* **2005**, *131*, 1199–1210. [CrossRef]
18. Roboski, J.; Finno, R.J. Distributions of ground movements parallel to deep excavations in clay. *Can. Geotech. J.* **2006**, *43*, 43–58. [CrossRef]
19. Hashash, Y.M.; Finno, R.J. Development of new integrated tools for predicting, monitoring, and controlling ground movements due to excavations. *Pract. Period. Struct. Des. Constr.* **2008**, *13*, 4–10. [CrossRef]
20. Ran, L.; Yi, T.H.; Ye, X.W.; Dong, X.B. Long-term deformation monitoring of metro-tunnel airshaft excavation during construction stage. *Int. J. Distrib. Sens. Netw.* **2012**, *8*, 972893. [CrossRef]
21. Yang, Y.; Lü, J.; Huang, X.; Tu, X. Sensor monitoring of a newly designed foundation pit supporting structure. *J. Cent. South Univ.* **2013**, *20*, 1064–1070. [CrossRef]
22. Zhang, H.B.; Chen, J.J.; Fan, F.; Wang, J.H. Deformation monitoring and performance analysis on the shield tunnel influenced by adjacent deep excavations. *J. Aerosp. Eng.* **2015**, *30*, B4015002. [CrossRef]
23. Li, X.; Zhang, L.; Jiang, S. Updating performance of high rock slopes by combining incremental time-series monitoring data and three-dimensional numerical analysis. *Int. J. Rock Mech. Min. Sci.* **2016**, *83*, 252–261. [CrossRef]
24. Qi, X.H.; Zhou, W.H. An efficient probabilistic back-analysis method for braced excavations using wall deflection data at multiple points. *Comput. Geotech.* **2017**, *85*, 186–198. [CrossRef]
25. Carlà, T.; Macciotta, R.; Hendry, M.; Martin, D.; Edwards, T.; Evans, T.; Farina, P.; Intrieri, E.; Casagli, N. Displacement of a landslide retaining wall and application of an enhanced failure forecasting approach. *Landslides* **2018**, *15*, 489–505. [CrossRef] [PubMed]
26. Christian, J.T. Geotechnical engineering reliability: How well do we know what we are doing? *J. Geotech. Geoenviron. Eng.* **2004**, *130*, 985–1003. [CrossRef]
27. Abdulai, M.; Sharifzadeh, M. Uncertainty and Reliability Analysis of Open Pit Rock Slopes: A Critical Review of Methods of Analysis. *Geotech. Geol. Eng.* **2019**, *37*, 1223–1247. [CrossRef]
28. Der Kiureghian, A.; Ditlevsen, O. Aleatory or epistemic? Does it matter? *Struct. Saf.* **2009**, *31*, 105–112. [CrossRef]
29. Sankararaman, S.; Mahadevan, S. Model validation under epistemic uncertainty. *Reliab. Eng. Syst. Saf.* **2011**, *96*, 1232–1241. [CrossRef]
30. Mullins, J.; Ling, Y.; Mahadevan, S.; Sun, L.; Strachan, A. Separation of aleatory and epistemic uncertainty in probabilistic model validation. *Reliab. Eng. Syst. Saf.* **2016**, *147*, 49–59. [CrossRef]
31. Engelund, S.; Rackwitz, R.; Lange, C. Approximations of first-passage times for differentiable processes based on higher-order threshold crossings. *Probabilistic Eng. Mech.* **1995**, *10*, 53–60. [CrossRef]
32. Melchers, R. *Structural Reliability Analysis and Prediction*; Wiley: New York, NY, USA, 1999.
33. Wang, C.; Zhang, H.; Beer, M. Structural time-dependent reliability assessment with new power spectral density function. *J. Struct. Eng.* **2019**, *145*, 04019163. [CrossRef]
34. Nakai, T.; Xu, L.; Yamazaki, H. 3D and 2D model tests and numerical analyses of settlements and earth pressures due to tunnel excavation. *Soils Found.* **1997**, *37*, 31–42. [CrossRef]

35. Gao, W.; Dou, Y.M.; Zhou, X.L.; Peng, F.L. Studies on displacements and earth pressures of pit-retaining structure during excavation by steps. *Chin. J. Geotech. Eng.* **2006**, *28*, 1455–1459.
36. Ou, C.Y. *Deep Excavation: Theory and Practice*; CRC Press: London, UK, 2014.
37. Boone, S.J. Design of Deep Excavations in Urban Environments. Ph.D. Thesis, University of Toronto, Toronto, Japan, 2004.
38. Hsiao, C.L. Wall and Ground Movements in a Braced Excavation in Clays and Serviceability Reliability of Adjacent Buildings. Ph.D. Thesis, Clemson University, Clemson, SC, USA, 2007.
39. Rice, S.O. Mathematical analysis of random noise. *Bell Syst. Tech. J.* **1944**, *23*, 282–332. [CrossRef]
40. Siegert, A.J. On the first passage time probability problem. *Phys. Rev.* **1951**, *81*, 617. [CrossRef]
41. Helstrom, C.; Isley, C. Two notes on a Markoff envelope process. *IRE Trans. Inf. Theory* **1959**, *5*, 139–140. [CrossRef]
42. Coleman, J.J. Reliability of aircraft structures in resisting chance failure. *Oper. Res.* **1959**, *7*, 639–645. [CrossRef]
43. Cramér, H. On the intersections between the trajectories of a normal stationary stochastic process and a high level. *Arkiv för Matematik* **1966**, *6*, 337–349. [CrossRef]
44. Schall, G.; Faber, M.H.; Rackwitz, R. The ergodicity assumption for sea states in the reliability estimation of offshore structures. *J. Offshore Mech. Arct. Eng.* **1991**, *113*, 241–246. [CrossRef]
45. Rackwitz, R. Computational techniques in stationary and non-stationary load combination—A review and some extensions. *J. Struct. Eng.* **1998**, *25*, 1–20.
46. Li, C.Q.; Melchers, R.E. Time-dependent reliability analysis of corrosion-induced concrete cracking. *ACI Struct. J.* **2005**, *102*, 543–549.
47. Hsiao, E.C.; Schuster, M.; Juang, C.H.; Kung, G.T. Reliability analysis and updating of excavation-induced ground settlement for building serviceability assessment. *J. Geotech. Geoenviron. Eng.* **2008**, *134*, 1448–1458. [CrossRef]
48. Cheney, W.; Light, W. *A Course in Approximation Theory*; Brooks/Cole Publishing Company: Pacific Grove, CA, USA, 2000.
49. Wang, C.; Li, Q.; Zou, A.; Zhang, L. A realistic resistance deterioration model for time-dependent reliability analysis of aging bridges. *J. Zhejiang Univ. Sci. A* **2015**, *16*, 513–524. [CrossRef]
50. Draper, N.R.; Smith, H. *Applied Regression Analysis*; John Wiley & Sons: Hoboken, NJ, USA, 1998.
51. Stark, T.D.; Choi, H. Slope inclinometers for landslides. *Landslides* **2008**, *5*, 339–350. [CrossRef]
52. Goh, A.; Wong, K.; Teh, C.; Wen, D. Pile response adjacent to braced excavation. *J. Geotech. Geoenviron. Eng.* **2003**, *129*, 383–386. [CrossRef]
53. Finno, R.J.; Calvello, M. Supported excavations: Observational method and inverse modeling. *J. Geotech. Geoenviron. Eng.* **2005**, *131*, 826–836. [CrossRef]
54. Peng, L. Data Processing System Development and Monitoring Results Analysis Methods Research of Borehole Inclinometer. Master's Thesis, Chengdu University of Technology, Chengdu, China, 2011.
55. Xiong, G.; Zhang, Q. Observation accuracy and applied study of inclinometer. *Hydro-Sci. Eng.* **1990**, *3*, 287–296. doi:10.16198/j.cnki.1009-640x.1990.03.007. [CrossRef]
56. Mikkelsen, P.E. Advances in inclinometer data analysis. In Proceedings of the Symposium on field Measurements in Geomechanics, FMGM, Oslo, Norway, 15–18 September 2003.